Journal of Solid State Chemistry **147,** 122–131 (1999)
Article ID jssc.1999.8184, available online at http://www.idealibrary.com on IDEAL®

Hydrothermal Synthesis, Powder Structural Determination, and Magnetic Study of the Novel Hydrated Iron Diphosphonate $[Fe_2(H_2O)_2(O_3P–CH_2–PO_3H)_2](H_2O)_2$ or MIL-13

M. Riou-Cavellec,*,[1] C. Serre,* J. Robino,* M. Noguès,† J.-M. Grenèche,‡ and G. Férey*

*Institut Lavoisier UMR CNRS 173 and †Laboratoire de Magnétisme et d'Optique de Versailles, 45 avenue des Etats-Unis, 78035 Versailles Cedex, France; and ‡Laboratoire de Physique de l'Etat Condensé, Faculté des Sciences, Université du Maine, Avenue O. Messiaen, 72085 Le Mans Cedex 9, France

Received October 13, 1998; accepted January 22, 1999

$[Fe_2(H_2O)_2(O_3P–CH_2–PO_3H)_2](H_2O)_2$ or MIL-13 was prepared hydrothermally (120 h at 473 K). Its structure was determined by powder X-ray diffraction. This compound crystallizes in the triclinic system (*P*-1) with the following cell parameters: $a = 9.8487(6)$ Å, $b = 8.0308(5)$ Å, $c = 9.9154(5)$ Å, $\alpha = 99.09(1)^\circ$, $\beta = 97.91(1)^\circ$, $\gamma = 89.38(1)^\circ$, $V = 766.97$ Å^3, $Z = 2$. Its bidimensional structure consists of $[Fe_2(H_2O)_2(O_3P–CH_2–PO_3H)_2]$ sheets, between which are located water molecules. The thermal study indicates that this compound undergoes several phase transitions. Moreover, this new iron diphosphonate shows a 2D antiferromagnetic behavior below 13(1) K, but remains paramagnetic at 4.2 K as shown by Mössbauer spectroscopy.

1. INTRODUCTION

Many organically templated compounds with open frameworks have been synthesized since the discovery of AlPO's in 1982 (1). In these phases, the microporous behavior should appear after extraction of the organic template, but in many cases the thermal treatment of these compounds induces the collapse of the structure. To avoid this difficulty, we have recently investigated some systems with chelating organic agents in order to complex the metal. This approach leads to new hybrid materials (MIL-*n* for Materials of Institute Lavoisier), where both organic and inorganic parts participate to the porous skeleton, with water molecules and/or ammonium cations located in the cavities. Using dicarboxylic acids or diphosphonic acids, our group succeeded in synthesizing new compounds with zeolitic character (2), cobalt (3), and rare-earth (4) diphosphonates with pillared structures. Since then, three-dimensional open framework vanadium diphosphonates have been discovered (MIL-2, MIL-3 (5) or MIL-5 (6)) with topologies different from those of metal diphosphonates already known in literature (7). A similar study was considered with iron as transition metal in order to get new magnetic open framework materials. A few iron phosphonates are already reported in literature (8–11), all are lamellar compounds such as the iron diphosphonate (MIL-13) described in this paper.

[1]To whom correspondence should be addressed.

EXPERIMENTAL

Synthesis

$[Fe_2(H_2O)_2(O_3P–CH_2–PO_3H)_2](H_2O)_2$ or MIL-13 was synthesized hydrothermally (under autogenous pressure). A mixture of $Fe_2O_3 : H_2O_3P–CH_2–PO_3H_2 : H_2O$ in the molar ratio 1 : 3 : 100 was kept at 473 K for 120 h in the 23-ml Teflon vessel of a Parr acid digestion bomb. After cooling to room temperature, the product was filtered off, washed with water, and air-dried. A white powder was obtained whose X-ray pattern ($\lambda_{CuK\alpha}$) is shown in Fig. 1. Scanning electron microscopy photography indicates a well-crystallized powder consisting of crystals of about 10 micrometers (Fig. 2).

Physical Methods

Energy dispersive X-ray spectrometry was performed on the title compound using a Jeol SM-5800LV scanning microscope equipped with an Oxford Instruments microanalysis system (Link Isis). Semi-quantitative EDX results indicated that the Fe/P atomic ratio was $\frac{1}{2}$.

The density value of MIL-13 was determined using a Micromeritics Accupyc 1330 pycnometer. Results gave 2.31 g/cm^{-3} (theoretical value 2.29 g/cm^{-3}).

The infrared absorption spectra (4000–200 cm^{-1}) were obtained using a Nicolet Magna IR550 spectrometer with the usual KBr pellet technique (Fig. 3). It confirmed the presence of P=O bonds (1190 cm^{-1}) and P–CH_2 bonds

0022-4596/99 $30.00

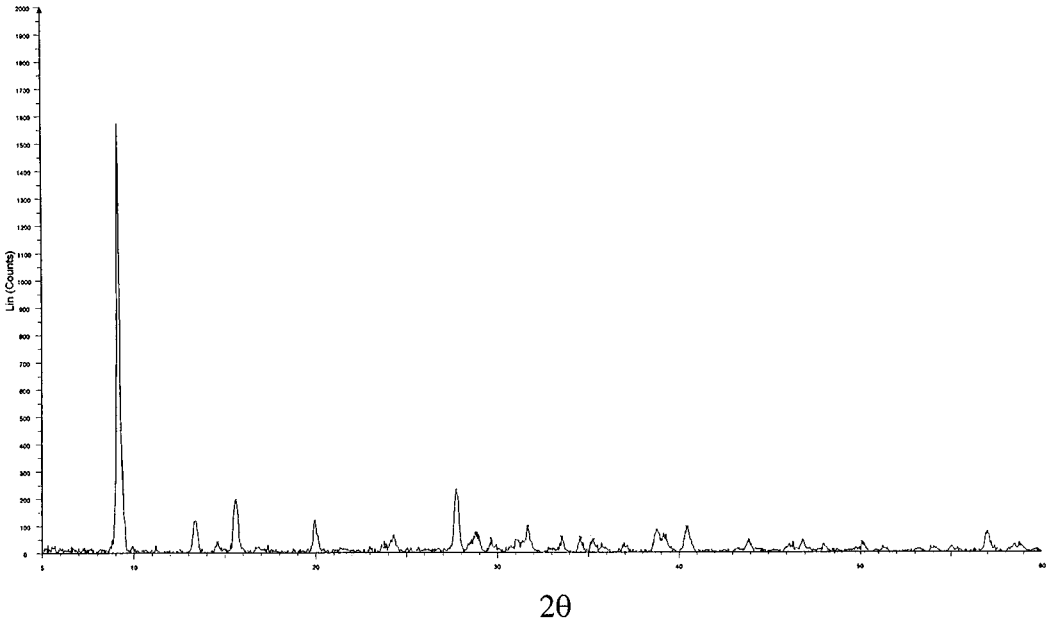

FIG. 1. X-ray experimental pattern of MIL-13.

(1367 and 794 cm^{-1}). A large peak in the range 3100–3200 cm^{-1} indicates the presence of water molecules (OH bonds).

TGA measurements were performed under O_2 atmosphere using a TA-Instrument type 2050 analyzer. The heating rate was 5°C/min from 30° to 600°C.

Thermodiffractometry carried out on the sample used a D5000 Siemens powder thermodiffractometer ($\lambda_{CoK\alpha}$) equipped with an Anton Parr furnace. The heating rate was 48°C/min with a 10°C step in the 30–600°C range.

Ab initio Powder Structural Determination

The title sample was first ground in ethanol using a MacCrone apparatus in order to homogenize the grain size,

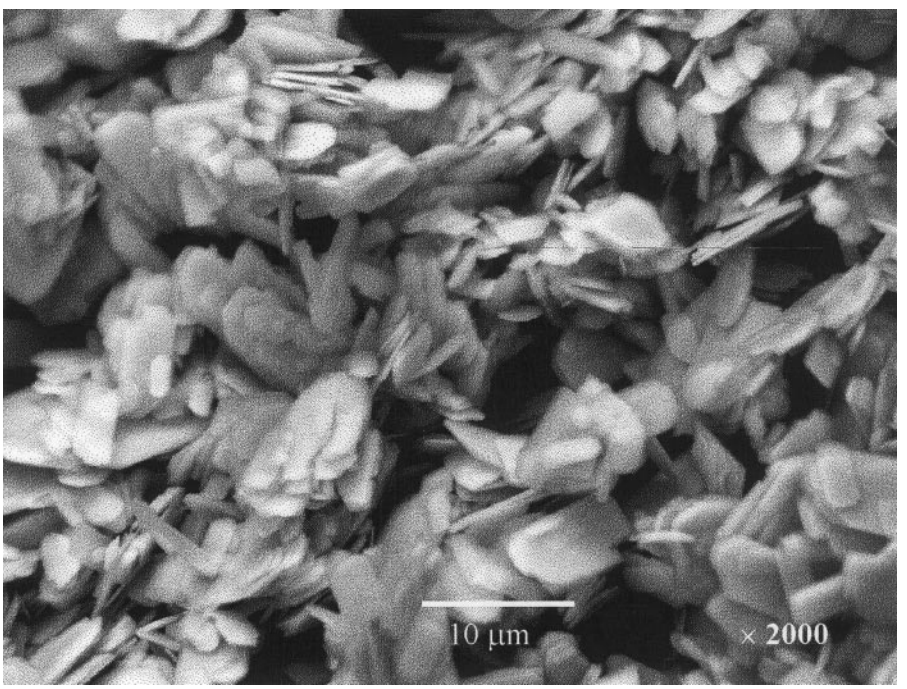

FIG. 2. Scanning electronic micrograph of MIL-13 showing a well-crystallized powder.

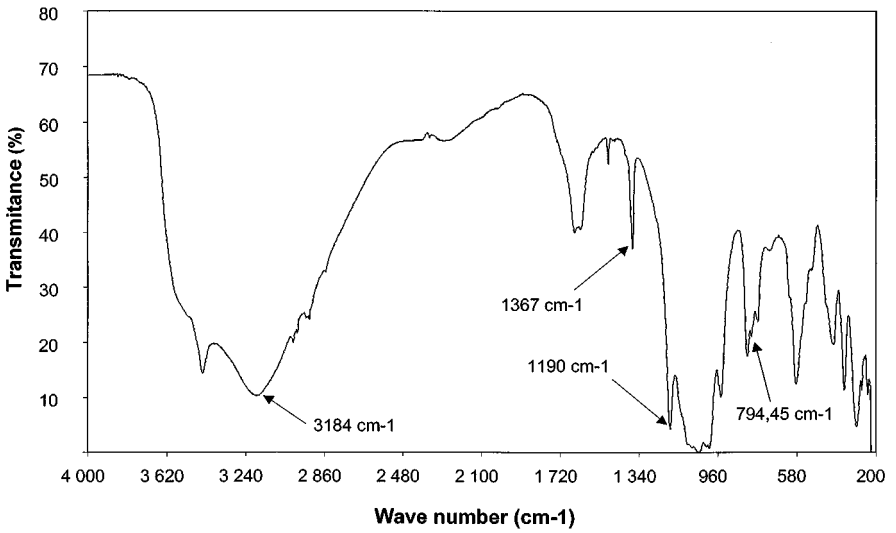

FIG. 3. IR spectrum of the title compound. We observed peaks at 1190 cm^{-1} (P=O bonds), at 1367–794 cm^{-1} (P–CH_2 bonds) and 3100–3200 cm^{-1} (OH bonds in water molecules).

and then it was introduced in a MacMurdie vertical-filling sample holder to limit preferential orientation effects. The diffraction pattern was collected on a D5000 Siemens diffractometer equipped with a secondary monochromator. The pattern was indexed with the DICVOL program (12). A triclinic solution was found with satisfactory figures of merit ($M(20)/F(20) = 24.2/47.9$ (0.0077, 54)). The space group was determined as P-1. The pattern matching was

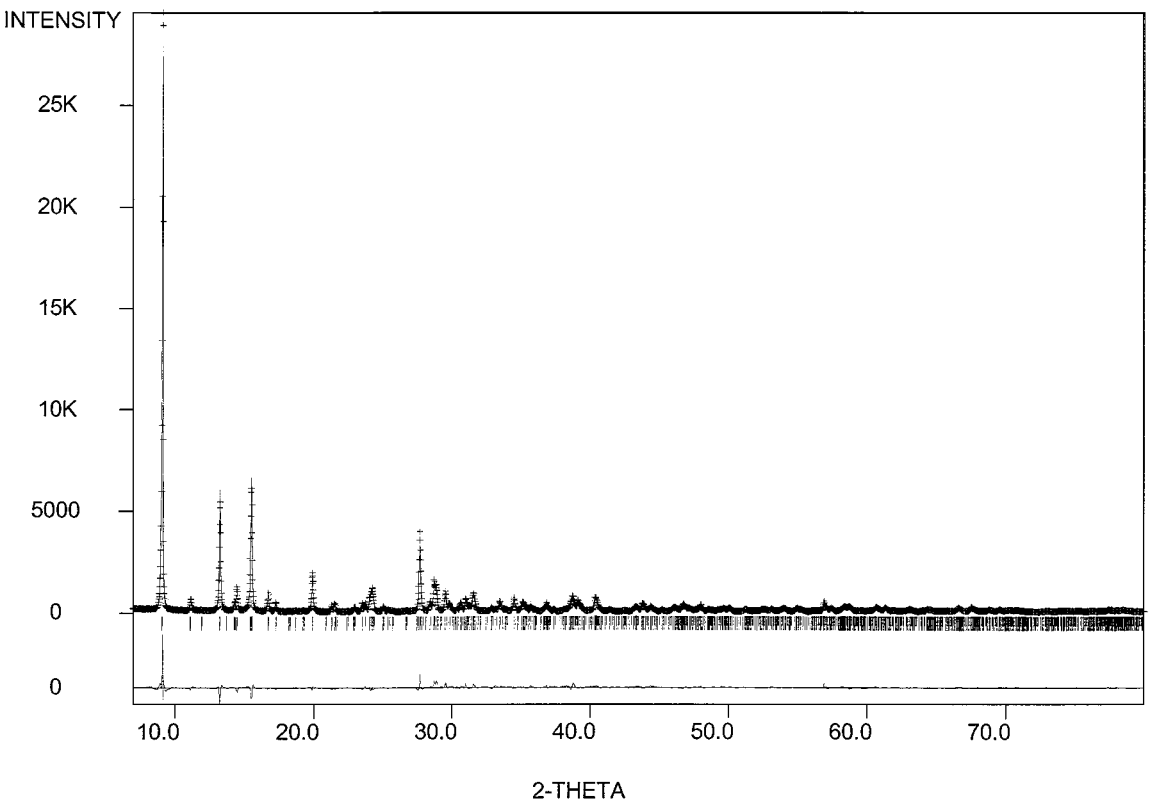

FIG. 4. Final Rietveld plot after X-ray powder structural resolution. The difference spectrum is given in the lower part at the same scale.

TABLE 1
Conditions of Data Measurements and Structure Refinement of MIL-13

Molar weight (g mol^{-1})	530
Calculated density (g cm^{-3})	2.29
Symmetry	Triclinic
Space group	*P*-1 (no. 2)
Multiplicity (*Z*)	2
a (Å)	9.849(1)
b (Å)	8.031(1)
c (Å)	9.915(1)
α (°)	99.089(1)
β (°)	97.910(1)
γ (°)	89.381(1)
V (Å^3)	766.98(1)
λ (λ_{Cu} (Å)): $K\alpha_1$ and $K\alpha_2$	1.54059, 1.54439
Data	h: $0 \rightarrow 8$, k: $-6 \rightarrow 6$, l: $-8 \rightarrow 8$
Ranges (°2θ)	$7.00 \rightarrow 42$ and $42.02 \rightarrow 80.0$
Time/step (s)	30 (range 1) and 60 (range 2)
Step size (°)	0.02
Total number of reflections	1871
Total number of points	3651
Number of parameters refined	96
Number of atoms refined	24
R_p (%)	10.5
R_{wp} (%)	13.4
R_{Bragg} (%)	7.14
R_F (%)	5.12

TABLE 2
Indexed Powder Pattern of MIL-13

h k l	2θ (°)	d_{hkl}	Int
001	9.112	9.697	100
010	11.148	7.930	2
0 −11	13.248	6.678	17
−110	14.303	6.187	1
110	14.461	6.120	3
011	15.499	5.713	21
1 −11	16.703	5.303	3
−111	17.261	5.133	2
0 −12	19.88	4.462	6
−210	21.261	4.176	1
201	21.472	4.135	2
−211	22.876	3.884	1
2 −11	23.467	3.788	1
−112	23.697	3.752	1
−202	24.012	3.703	2
−1 −21	24.224	3.671	3
1 −21	24.986	3.561	1
202	27.646	3.224	15
−1 −13	28.389	3.141	2
2 −12	28.669	3.111	4
−220	28.835	3.094	4
−3 −11	29.485	3.027	4
310	29.788	2.997	1
2 −21	29.976	2.979	1

Note. The indexing is based on a triclinic cell with the dimensions $a = 9.849$ (1) Å, $b = 8.031$ (1) Å, $c = 9.915$ (1) Å, $\alpha = 99.09°$ (1), $\beta = 97.91°$ (1), $\gamma = 89.38°$ (1), S.G. *P*-1 (no. 2).

TABLE 3
Atomic Coordinates

Fe1	0.5903 (1)	− 0.2073 (1)	0.1546 (8)
Fe2	0.0880 (1)	− 0.2219 (1)	0.1591 (8)
P1	0.8628 (1)	0.0302 (1)	0.3095 (1)
P2	0.8097 (1)	− 0.0680 (1)	0.0057 (1)
P3	0.6800 (1)	− 0.5680 (1)	− 0.0217 (1)
P4	0.6234 (1)	− 0.6197 (4)	− 0.3063 (1)
O1	0.325 (2)	− 0.561 (3)	− 0.103 (2)
O2	0.667 (3)	− 0.119 (3)	0.008 (2)
O3w	0.998 (3)	− 0.543 (3)	− 0.173 (3)
O4	0.917 (2)	− 0.219 (3)	0.021 (3)
O5	0.805 (3)	− 0.001 (3)	− 0.125 (2)
O6	− 0.043 (2)	− 0.103 (3)	0.270 (2)
O7	0.499 (3)	− 0.736 (3)	− 0.296 (2)
O8	0.835 (2)	− 0.628 (3)	0.015 (2)
O9	0.419 (2)	− 0.277 (3)	0.012 (2)
C1	0.852 (5)	0.096 (4)	0.148 (2)
C2	0.353 (5)	0.444 (3)	0.159 (2)
O10 (H)	0.860 (3)	0.134 (3)	0.463 (2)
O11	0.252 (2)	0.733 (3)	0.297 (2)
O12	0.752 (2)	0.887 (3)	0.286 (2)
O13w	0.517 (3)	0.059 (3)	0.194 (2)
O14 (H)	0.359 (3)	0.553 (4)	0.459 (2)
Ow1	0.851 (3)	0.528 (3)	0.368 (2)
Ow2	0.346 (3)	0.182 (3)	0.412 (2)

Note. The index *w* is added for a water molecule. O_i(H) means that it is a hydroxyl group. Ow1 and Ow2 are interlayered water molecules.

TABLE 4
Principal Bond Distances (Å) in MIL-13

(Fe1)–(O1):	2.08 (2)
(Fe1)–(O2):	1.98 (2)
(Fe1)–(O7):	1.87 (2)
(Fe1)–(O9):	2.06 (2)
(Fe1)–(O12):	1.99 (2)
(Fe1)–($O13_w$):	2.24 (3)
(Fe2)–($O3_w$):	2.09 (3)
(Fe2)–(O4):	2.02 (3)
(Fe2)–(O5):	2.18 (3)
(Fe2)–(O6):	1.95 (3)
(Fe2)–(O8):	2.17 (2)
(Fe2)–(O11):	2.04 (2)
(P1)–(O6):	1.45 (3)
(P1)–($O10_H$):	1.62 (3)
(P1)–(O12):	1.56 (3)
(P1)–(C1):	1.76 (2)
(P2)–(O2):	1.48 (3)
(P2)–(O4):	1.61 (3)
(P2)–(O5):	1.47 (3)
(P2)–(C1):	1.78 (3)
(P3)–(O1):	1.45 (2)
(P3)–(O8):	1.61 (3)
(P3)–(O9):	1.61 (3)
(P3)–(C2):	1.81 (3)
(P4)–(O7):	1.57 (3)
(P4)–(C2):	1.85 (3)
(P4)–(O11):	1.54 (3)
(P4)–($O14_H$):	1.71 (3)

adjusted with FULLPROF 97 (13), the structure was then solved by direct method using SIRPOW 92 (14). Mean distance constraints were applied during the refinement: (Fe–O) = 1.95 Å, (P–O) = 1.55 Å, (P–C) = 1.82 Å. An overall thermal factor applied to all atoms was refined. The final agreement factors are quite satisfactory: $R_p = 10.5\%$, $R_{wp} = 13.4\%$ (nonconventionnal Rietveld factors), and $R_{Bragg} = 7.14\%$, $R_F = 5.12\%$. The corresponding Rietveld plot is given in Fig. 4.

The conditions of data measurements and structure refinement of MIL-13 are summarized in Table 1. The d_{hkl} values are indicated in Table 2. The atomic coordinates and principal bond distances are given in Tables 3 and 4, respectively. Principal angles are given in the Appendix.

Magnetic Measurements and Mössbauer Study

The magnetization M of the sample was measured as a function of the applied field H ($H = 0.9$ T) at many temperatures in the range 4 to 300 K with a SQUID (Quantum Design Squid Device) apparatus. The resulting magnetic susceptibility ($\delta M/\delta H$) was deduced.

Mössbauer experiments were carried out at 300, 77, and 4.2 K using a constant acceleration spectrometer and a ^{57}Co source diffused into a Rh matrix. The isomer shift values are quoted relative to α-Fe foil at 300 K. The hyperfine parameters were refined using a least-square fitting procedure in MOSFIT program (15).

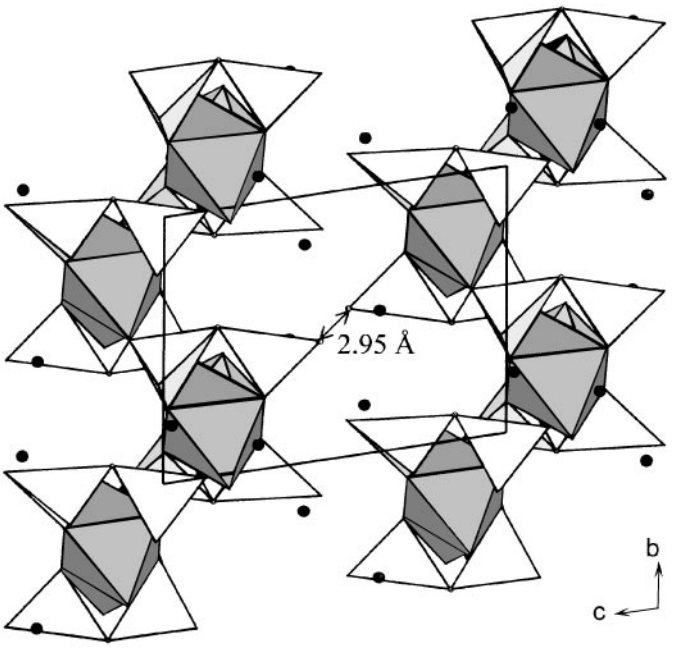

FIG. 5. Projection of MIL-13 showing the bidimensional character of the structure. Diphosphonic ions are represented as double tetrahedra linked via a C atom. Water molecules Ow1 and Ow2 (in black) are located between the corrugated planes. The shorter interlayer distance (O_{14H}–O_{14H}) is 2.95 Å.

RESULTS AND DISCUSSION

MIL-13 is a layered compound. Its corrugated sheets have a $[Fe_2(H_2O)_2(O_3P–CH_2–PO_3H)_2]$ stoichiometry.

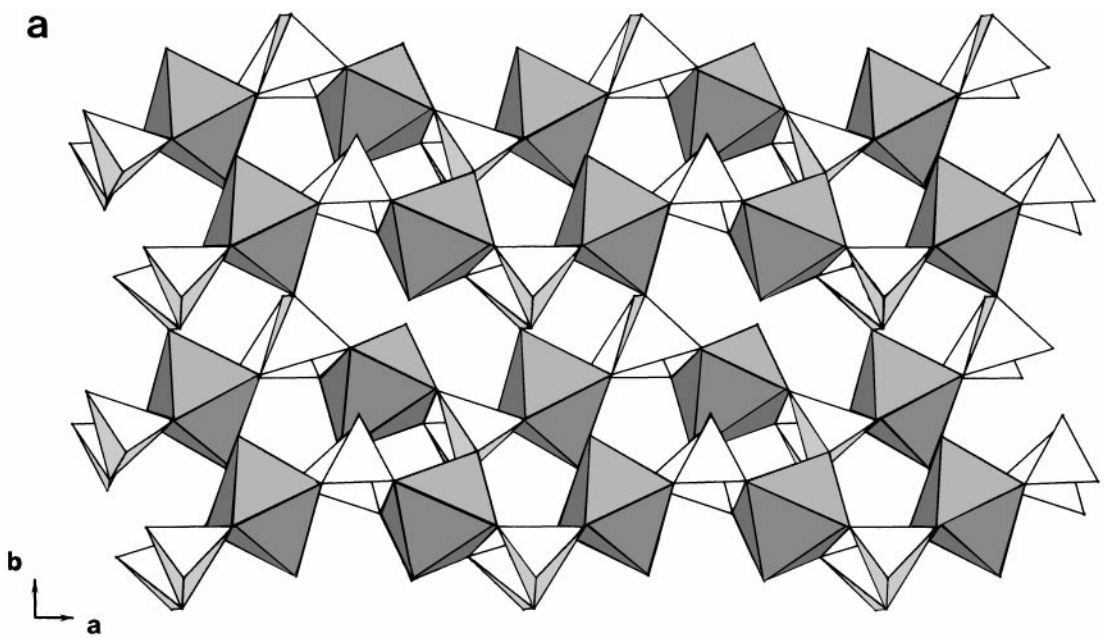

FIG. 6. (a) Projection of a hybrid organic–inorganic layer. Isolated $[FeO_5(H_2O)]$ octahedra are chelated by $[HO_3P–CH_2–PO_3]$ units. The free vertex of each octahedron corresponds to the water molecule. (b) Representation of the tilted chain.

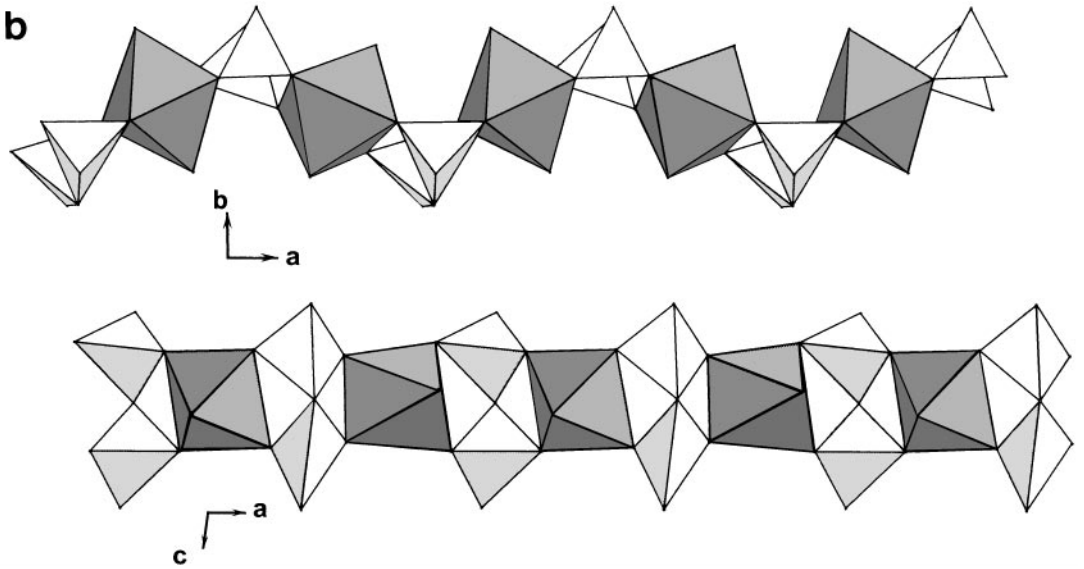

FIGURE 6—*Continued*

Water molecules O_{w1} and O_{w2} are inserted in between the layers (Fig. 5). The shortest distance between two consecutive corrugated planes is 2.95 Å (i.e, $O14_H$–$O14_H$), whereas the distance between two consecutive layers correspond to the *c* parameter of the cell.

The mixed organic–inorganic layer (Fig. 6a) can be described as the connection of tilted chains represented in Fig. 6b. Each chain is built up from the bonding of isolated iron octahedra [Fe(1,2)$O_5(H_2O)$] with a water molecule in terminal position (O_{13w} and O_{3w}, respectively) and [HO_3P–CH_2–PO_3] units. A [HO_3P–CH_2–PO_3] unit results from the connection of two [PO_3(H)] tetrahedra via the CH_2 vertex (analogy with P_2O_7 diphosphate unit is obvious); in this unit, one of the tetrahedra has an apex in

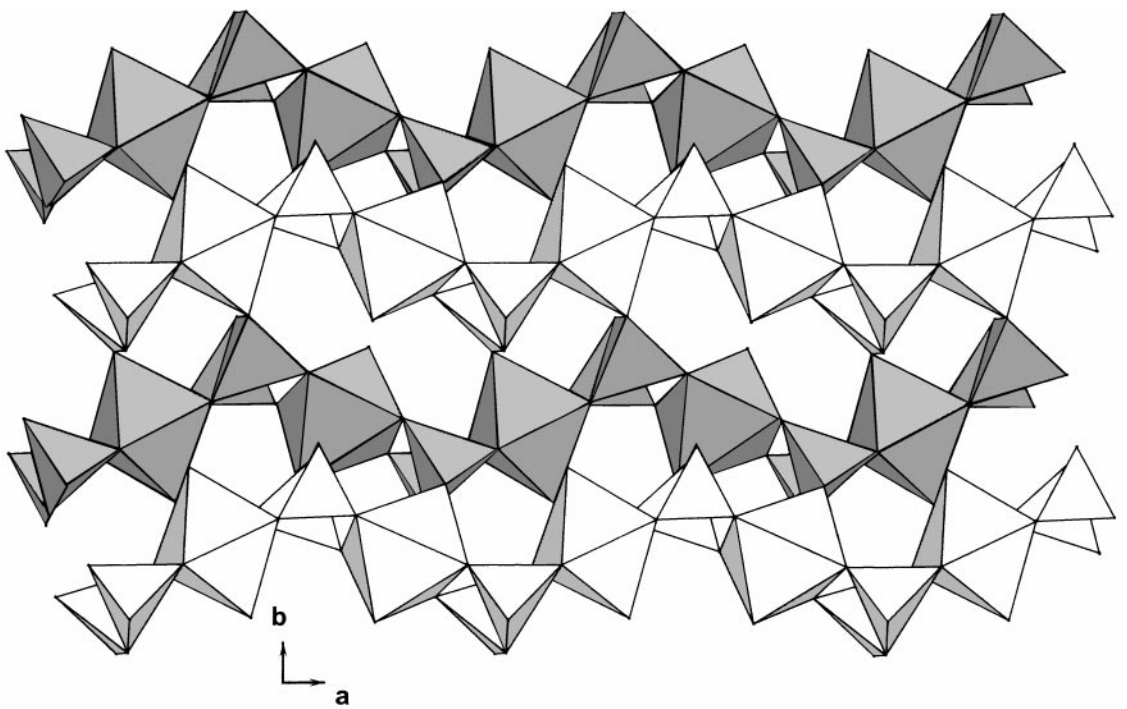

FIG. 7. Connection of tilted chains. In the sheet, each octahedron is linked to three methylenediphosphonic units.

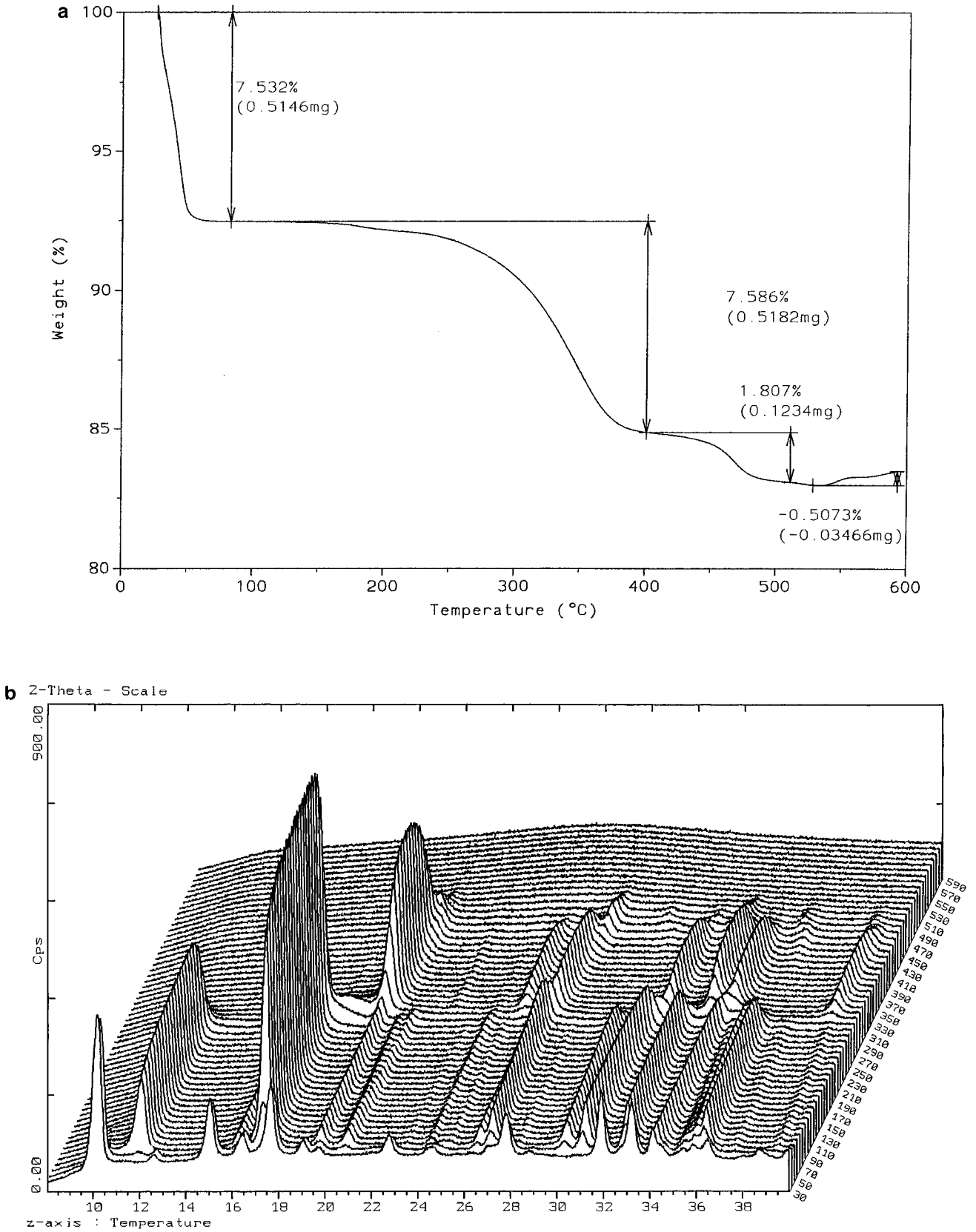

FIG. 8. (a) Thermogravimetric curve of MIL-13 indicating three weight losses. (b) Thermodiffractogram of MIL-13 showing three transition phases.

a terminal position that corresponds to a hydroxyl group [$HO_3P(1,4)$–CH_2–$P(2,3)O_3$]. This is confirmed by bond valence calculations (16), which also indicate the trivalent state of iron. Within the chain, each iron octahedron is linked to two chelatant [HO_3P–CH_2–PO_3] units (Fig. 6b). These tilted chains are connected in such a way that each iron octahedron is linked to three [HO_3P–CH_2–PO_3] units: the two chelatant groups previously described within the tilted chain and one more bonding [HO_3P–CH_2–PO_3] unit belonging to a neighboring chain (Fig. 7). These connections lead to the formation of the corrugated planes. One can notice eight-membered apertures within the layer, inside which point the free apices of iron octahedra.

In Fig. 8a, the thermogravimetric analysis curve (TGA) of MIL-13 indicates three weight losses that is very consistent with the thermodiffractogram of the title compound (Fig. 8b). The first weight loss ($\%_{exp} = 7.53$) which occurs in the 30–50°C temperature range corresponds to the dehydration ($\%_{theo} = 6.8$) of $[Fe_2(H_2O)_2(O_3P$–CH_2–$PO_3H)_2](H_2O)_2$. This dehydration is reversible but slow; it probably concerns the departure of water molecules located in the interlamellar space. On the thermodiffractogram, we observed the hydrated phase, i.e., $[Fe_2(H_2O)_2(O_3P$–CH_2–$PO_3H)_2](H_2O)_2$ in the 30–40°C range; beyond, the dehydrated phase, i.e., $[Fe_2(H_2O)_2(O_3P$–CH_2–$PO_3H)_2]$, stands until 280°C. Then, by TGA, we observed a second weight loss ($\%_{exp} = 7.58$) involving the second phase transition occurring on the thermodiffractogram at about 280°C. To explain this second loss, we can suggest the departure of the terminal water molecules of the iron octahedra ($\%_{theo} = 6.8$), so that each ferric ion would become fivefold coordinated.

We are now carrying out Mössbauer experiments as a function of temperature in order to underline a possible environmental change of ferric ions. This is currently in progress just as we are trying to solve the structure of the phase appearing in the 280C–460°C range.

The third weight loss indicated by TGA is around 460°C ($\%_{exp} = 1.8$); on the thermodiffractogram, it then appears as the third transition phase leading to an amorphous phase. This latest loss might involve the departure of CH_2 groups

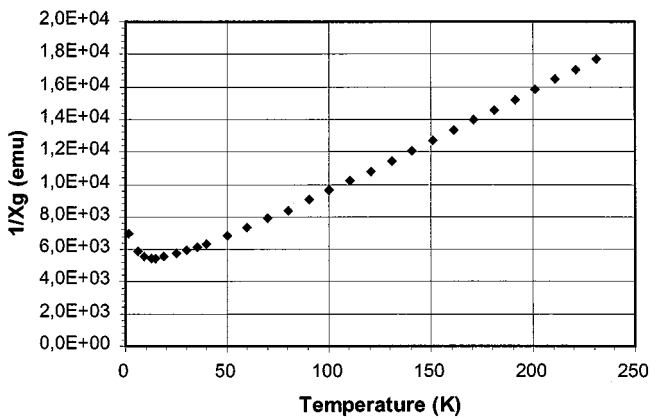

FIG. 9. Thermal behavior of the magnetic susceptibility of MIL-13 exhibiting, at first glance, antiferromagnetic behavior.

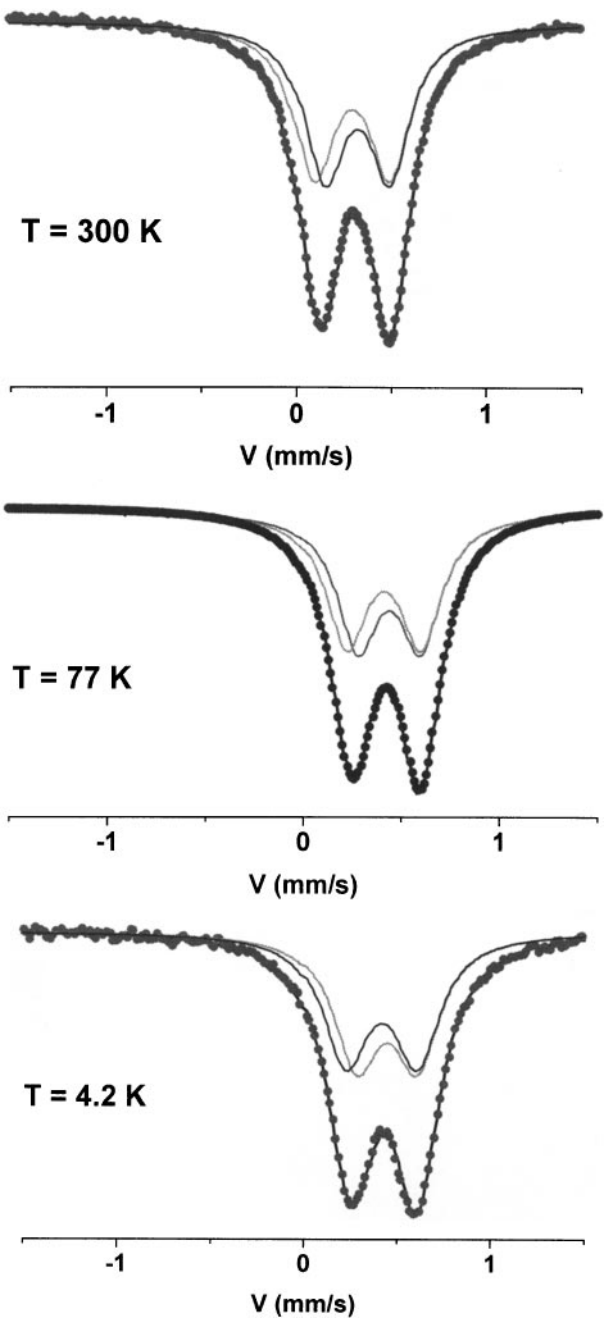

FIG. 10. Mössbauer spectra at 300, 77, and 4.2 K. The title compound remains paramagnetic in the whole range of temperature (two quadrupolar doublets appear on each spectrum).

in the (O_3P–CH_2–PO_3H) unities, but it is probably not a satisfying explanation.

The inverse magnetic susceptibility reported in Fig. 9 shows that MIL-13 exhibits a minimun at 13(1) K, which could be considered at first glance an antiferromagnetic ordering. However, Mössbauer spectroscopy will show a paramagnetic behavior down to 4.2 K

The Mössbauer spectra recorded on MIL-13 at 300, 77, and 4.2 K are represented in Fig. 10. Whatever the temperature, the Mössbauer spectra exhibit an asymmetric doublet with sharp lines. The hyperfine structure is consistent with a paramagnetic state even at 4.2 K.

We have first checked that the asymmetry is not only due to a texture effect after recording with the magic angle configuration. All these spectra can be described by at least two quadrupolar components according to the crystallographic predictions. We assume the presence of two equiprobable iron sites. The hyperfine parameters, which are listed in Table 5, indicate the presence of two high-spin state Fe^{3+} ions in agreement with previous valence calculations. The values of isomer shift and quadrupolar splitting are slightly different in agreement with the slight difference existing between the average Fe^{3+}–O distances (mean Fe(1)–O distance is 2.037 Å, whereas mean Fe(2)–O is 2.075 Å) and calculated distortions (17) for Fe(1) and Fe(2) octahedra, which are, respectively, $\Delta_1 . 10^4 = 53.5$ and $\Delta_2 . 10^4 = 15.8$. These structural considerations allow us to assign each quadrupolar component to an iron crystallographic site: Γ_1 corresponds to Fe(1) and Γ_2 to Fe(2) (the higher is the distortion, the larger the quadrupolar splitting).

The difference between magnetic behavior observed by magnetization measurements and Mössbauer experiments is probably due to a 2D magnetic behavior. Indeed, according to the structure of the compound, we expect a 2D magnetic ordering within sheets, but no magnetic interactions between layers, the latter being too weak. This is probably why we do not observe two magnetic sextets by Mössbauer spectroscopy at 4.2 K. This has to occur at a temperature lower than 4.2 K.

TABLE 5
Hyperfine Parameters at 300, 77, 4.2 K

		IS (mm/s) ± 0.02	GA (mm/s) ± 0.02	SQ (mm/s) ± 0.02	%
300 K	Γ_1	0.42	0.13	0.40	50
	Γ_2	0.45	0.13	0.34	50
77 K	Γ_1	0.53	0.13	0.38	50
	Γ_2	0.55	0.13	0.32	50
4.2 K	Γ_1	0.53	0.29	0.38	50
	Γ_2	0.56	0.29	0.32	50

APPENDIX

Principal Angles in $[Fe_2(H_2O)_2(O_3P–CH_2–PO_3H)_2](H_2O)_2$

(O1)–(Fe1)–(O2):	91.4 (2)
(O1)–(Fe1)–(O7):	97.4 (2)
(O1)–(Fe1)–(O9):	90.4 (2)
(O1)–(Fe1)–(O12):	95.1 (2)
(O1)–(Fe1)–(O13):	170.8 (2)
(O2)–(Fe1)–(O9):	86.2 (2)
(O2)–(Fe1)–(O12):	89.6 (2)
(O2)–(Fe1)–(O13):	80.2 (2)
(O7)–(Fe1)–(O9):	90.9 (2)
(O7)–(Fe1)–(O12):	92.4 (2)
(O7)–(Fe1)–(O13):	91.1 (2)
(O9)–(Fe1)–(O12):	173.2 (2)
(O9)–(Fe1)–(O13):	91.4 (2)
(O12)–(Fe1)–(O13):	82.6 (2)
(O3)–(Fe2)–(O4):	81.2 (2)
(O3)–(Fe2)–(O5):	171.3 (2)
(O3)–(Fe2)–(O6):	91.9 (2)
(O3)–(Fe2)–(O8):	80.9 (2)
(O3)–(Fe2)–(O11):	89.2 (2)
(O4)–(Fe2)–(O5):	100.5 (2)
(O4)–(Fe2)–(O6):	77.0 (2)
(O4)–(Fe2)–(O8):	82.5 (2)
(O4)–(Fe2)–(O11):	170.2 (2)
(O5)–(Fe2)–(O6):	96.7 (2)
(O5)–(Fe2)–(O8):	90.8 (2)
(O5)–(Fe2)–(O11):	88.7 (2)
(O6)–(Fe2)–(O8):	159.2 (2)
(O6)–(Fe2)–(O11):	105.3 (2)
(O8)–(Fe2)–(O11):	94.2 (2)
(O6)–(P1)–(C1):	91.2 (2)
(O6)–(P1)–(O10):	126.5 (3)
(O6)–(P1)–(O12):	86.0 (2)
(C1)–(P1)–(O10):	132.0 (2)
(C1)–(P1)–(O12):	103.6 (2)
(O10)–(P1)–(O12):	107.2 (2)
(O2)–(P2)–(O4):	114.2 (3)
(O2)–(P2)–(O5):	102.9 (3)
(O2)–(P2)–(C1):	106.7 (3)
(O4)–(P2)–(O5):	114.3 (3)
(O4)–(P2)–(C1):	108.0 (2)
(O5)–(P2)–(C1):	110.4 (2)
(O1)–(P3)–(O8):	97.3 (2)
(O1)–(P3)–(O9):	109.5 (3)
(O1)–(P3)–(C2):	102.0 (2)
(O8)–(P3)–(O9):	107.0 (2)
(O8)–(P3)–(C2):	116.3 (3)
(O9)–(P3)–(C2):	121.4 (2)

(O7)–(P4)–(C2):	111.3 (3)
(O7)–(P4)–(O11):	104.2 (3)
(O7)–(P4)–(O14):	120.9 (3)
(C2)–(P4)–(O11):	108.4 (3)
(C2)–(P4)–(O14):	112.4 (2)
(O11)–(P4)–(O14):	97.6 (2)

REFERENCES

1. S. T. Wilson, B. M. Lok, C. A. Messina, T. R. Cannan, and E. M. Flanigen, *J. Am. Chem. Soc.* **104,** 1146 (1982).
2. F. Serpaggi and G. Férey, *J. Mater. Chem.* **8,** 2737 (1998).
3. C. Livage, C. Egger, M. Nogues, and G. Férey, *J. Mater. Chem.* **8,** 2743 (1998).
4. F. Serpaggi and G. Férey, *J. Mater. Chem.* **8,** 2749 (1998).
5. D. Riou, O. Roubeau, and G. Férey, *Microporous Mesoporous Mater.* **23,** 23 (1998).
6. D. Riou, C. Serre, and G. Férey, *J. Solid State Chem.* **141,** 89 (1998).
7. D. L. Lohse and S. C. Sevov, *Angew. Chem. Int. Ed. Engl.* **36,** 1619 (1997) and references therein; V. Soghomonian, Q. Chen, R. C. Haushalter, and J. Zubieta, *Angew. Chem. Int. Ed. Engl.* **34,** 223 (1995) and references therein; P. J. Zapf, D. J. Rose, R. C. Haushalter, and J. Zubieta, *J. Solid State Chem.* **125,** 182 (1996); S. Drumel, P. Janvier, D. Deniaud, and B. Bujoli, *J. Chem. Soc. Chem. Commun.* 1051 (1995).
8. P. Palvadeau, M. Queignec, J. P. Venien, B. Bujoli, and J. Villieras, *Mater. Res. Bull.* **23**, 1561 (1988).
9. B. Bujoli, P. Palvadeau, and J. Rouxel, *C. R. Acad. Sci. Paris* **310,** 1213 (1990).
10. B. Bujoli, P. Palvadeau, and J. Rouxel, *Chem. Mater.* **2,** 582 (1990).
11. B. Bujoli, O. Pena, P. Palvadeau, J. Le Bideau, C. Payen, and J. Rouxel, *Chem. Mater.* **5,** 583 (1993).
12. A. Boultif and D. Louër, *J. Appl. Crystallogr.* **24,** 987 (1991).
13. J. Rodriguez-Carjaval, "Collected Abstracts of Powder Diffraction Meeting," Vol. 127. Toulouse, France, 1990.
14. A. Altomare, M. C. Burla, M. Camalli, G. Cascarano, C. Giacovazzo, A. Guagliardi, and G. Polidori, *J. Appl. Crystallogr.* **27,** 435 (1992).
15. J. Teillet and F. Varret, Mosfit Program (Université du Maine), unpublished.
16. N. E. Brese and M. O'Keefe, *Acta Crystallogr. B* **47,** 192 (1991).
17. R. D. Shannon, *Acta Crystallogr. Sect. A* **32,** 751 (1976).